Lossless 1×4 Silicon Photonic ROADM based on a Monolithic Integrated Erbium Doped Waveguide Amplifier on a Si_3N_4 platform

C. Vagionas, A. Tsakyridis, T. Chrysostomidis, I. Roumpos, K. Fotiadis, A. Manolis, J. Mu, M. Dijkstra, S.M. Garcia Blanco, R. M. Oldenbeuving, P. W. L. van Dijk, C. G.H. Roeloffzen, K. Vyrsokinos, N. Pleros, T. Alexoudi

(Top scored)

***Abstract*— During the past years, incorporating Optical Circuit Switches (OCS) in high-bandwidth optical interconnects has outlined the critical challenges of achieving ultra-low fiber-to-fiber losses (FtF) and constantly decreasing costs for Photonic Integrated Circuits (PICs). This work aims to simultaneously satisfy both the low-loss and low-cost requirements by bringing two of the most successful example-technologies in the history of optics, i.e. EDFAs and ROADMs to a common Si_3N_4 platform. In particular, the proof-of-concept operation of a lossless four-port Silicon Photonic (SiPho) ROADM is experimentally presented for the first time based on two PIC prototypes on a Si_3N_4 platform, including a monolithic-integrated 5.9 cm-long spiral $Al_2O_3:Er^{3+}$ Erbium Doped Waveguide Amplifier (EDWA) with 15 dB signal enhancement capabilities and a lattice MZI-interleaver ROAM layout with 100 GHz channel spacing. Considering an ultra-low 2.55 dB FtF loss of the ROADM along with 0.5 dB loss for each of the two coupling-interfaces between the Si_3N_4 and $Al_2O_3:Er^{3+}$ waveguide layers, a cumulative loss of 3.55 dB is obtained, which can be compensated by the 3.6 dB net gain provided by the EDWA to four incoming WDM signals of -1.7 dBm/channel. Lossless wavelength-routing operation is validated at up to 240 Gb/s WDM (4λ × 60Gb/s) data traffic, while the cascadability of the proposed device is benchmarked in a realistic two-stage optical bus topology with 10 km single mode fiber that selectively routes 4λ × 25Gb/s WDM data channels to any of its eight Drop output ports. This work forms the first demonstration of lossless ROADM operation exclusively on SiPho technology, highlighting a promising roadmap for large scale SiPho switching matrices and more complex PICs co-integrated with EDWAs.**

***Index Terms*—Optical Switching, ROADM, Silicon Photonics, Optical Amplifiers, Optical Networks, Wavelength Routing**

I. Introduction

THE rise of cloud-based applications during the last decade comes along with a growing demand for high bandwidth interconnectivity at Data Centers (DCs) and Metro-Access [1], expected to continue to grow in the forthcoming era of the Internet of Things (IoT) and 5G [2]. Meanwhile, optical line rates are scaling beyond 100 Gb/s/λ [3], constantly pushing for more efficient optical routing and switching functionalities [4]. To date, fiber-optical networks rely mostly on Wavelength Division Multiplexing (WDM) techniques for transmitting multiple channels across a long distance [1], while Erbium Doped Fiber Amplifiers (EDFAs) form the most dominant amplification technology featuring long-validated high-gain, high-linearity, low-noise aspects and applications ranging from short reach and metro to ultralong-haul links [5].

In WDM optical networks, Reconfigurable Optical Add Drop Multiplexers (ROADMs) realize wavelength-selective cross-connect (WXC) functionality with dynamic light path reconfiguration [6]. Allowing to Add, Drop or pass-Through any specific wavelength of a WDM stream transparently and independently of the linerate, ROADMs and Optical Circuit Switches (OCSs) can handle the scaling of optical linerates without any additional power-consumption [10], as opposed to electronics switches, which sacrifice energy-consumption for higher speed. Hence, photonic switching started to penetrate various network segments, including DCs environments [8][9], transport [10][11] and 5G fronthaul [12]-[15], bringing dynamic network provisioning at reduced size or cost.

Nevertheless, incorporating OCSs and ROADMs in the network has outlined two of the most critical challenges, i.e., to maintain ultra-low Fiber-to-Fiber (FtF) losses and constantly decreasing costs, in order to simultaneously meet the scalability requirement to high-port counts or multi-stage operation [16]-[18] while being in-line with electronic-photonic integration roadmaps for cost-effective optical interconnects [19][20]. Traditionally, OCSs and ROADMs deploy Micro-electro Mechanical Systems (MEMs) or piezoelectric actuators

Manuscript received Month XX, 2021; revised Month XX, 2021; accepted Month XX, 2021. Date of publication Month XX, 2021; date of current version Month XX, 2021. The work has received funding from the Hellenic Foundation for Research and Innovation (HFRI) and the General Secretariat for Research and Technology (GSRT), through the CAM-UP project under grant agreement No 230 and the ORION project (No 585) and from the Stichting voor de Technische Wetenschappen (STW) (STW-13536) and in part by the European Research Council (ERC) under European Union's Horizon 2020 Research and Innovation Program under Agreement 648978.

C. Vagionas, A. Tsakyridis, K. Fotiadis, A. Manolis, N. Pleros and T. Alexoudi are with the Department of Informatics and Center for Interdisciplinary Research and Innovation, Aristotle University of Thessaloniki, 57001, Greece. (e-mail: chvagion@csd.auth.gr))

T. Chrysostomidis, I. Roumpos and K. Vyrsokinos are with the Department of Physics and Center for Interdisciplinary Research and Innovation, Aristotle University of Thessaloniki, 57001, Greece

J. Mu, M. Dijkstra, and S.M. Garcia Blanco are with the Integrated Optical Systems (IOS) Group, MESA+ Institute for Nanotechnology, University of Twente, P.O Box 217, 7500 AE, Enschede, The Netherlands

R. M. Oldenbeuving, P. W. L. van Dijk, C. G.H. Roeloffzen are with LIONIX International B.V., Enschede, The Netherlands

that assemble discrete components with free-space alignment schemes. On the other hand, advanced CMOS industry, relying on mature integration processes, has stimulated a rapid growth of the Silicon Photonics (SiPho) ecosystem, including SiPho switches, bearing promises for a cost-effective solution with large integrability [4]-[8]. Yet, SiPho switches need to overcome the high fiber-to-fiber insertion and propagation losses, typically above >10 dB even for small port-counts [4],[8]-[17], while accumulating to prohibitively high values when cascading multiple stages.

Towards scalable photonic switching and wavelength routing functionalities, optical amplification elements need to be integrated with the switching matrix. Owing to the direct bandgap and inherent stimulated emission of III-V materials, early prototypes of lossless OCSs were integrating several Semiconductor Optical Amplifiers (SOAs) in 4×4 [21], 8×8 [22] and 16×16 [18] layouts on InP platform for nearly two decades and are more recently proposed as Add/Drop switches in Metro networks with channel-rates up to 40 Gb/s [24][25]. Towards bridging the gain-properties of III-V materials with the large-integrability and cost-benefits of SiPho, arrays of SOAs can be hybridly-integrated next to SiPho switching matrices for DCs, demonstrating 4×4 [26] and 8×8 port counts [7][27][28] with up to 33 Gbd channel-rates. Yet, hybrid-integration requires challenging assembly processes to align and bond dies of two different waveguide platforms, resulting in increased complexity and lower device yield [8],[29]-[32], while most importantly SOAs induce non-linear distortions and inter-channel cross-talk between multiple WDM data-streams, which may severely degrade the signal quality [7], the input dynamic range [27] and multiple channel-operation [33].

Erbium Doped Waveguide Amplifiers (EDWAs) and rare earth materials have made significant progress during the last decade [34]-[38]. Monolithically integrating aluminum oxide as host platform on top of SiPho waveguides, profound EDWA prototypes have unraveled broadband optical amplification across 70 nm spectrum, gain values up to 18 dB, as well as large dynamic range of more than 20 dB [35]. Yet, still these tremendous benchmarks have been validated mostly in single-channel transmission at data rates up to 170 Gb/s [38], thus not being deployed so far in larger circuitries that could pave the way for lossless, monolithic SiPho switching matrices.

The current work envisions bridging this gap by presenting for the first time a lossless ROADM-node architecture built exclusively on a Si_3N_4 platform. The proposed ROADM comprises a 5.9 cm-long spiral $Al_2O_3:Er^{3+}$ EDWA monolithically integrated on top of a Si_3N_4 waveguide followed by a 1×4 Mach Zehnder Interferometer (MZI)-based ROADM configuration-layout with 100 GHz channel spacing. The proof of concept operation relies on two Photonic Integrated Circuit (PIC) components both fabricated on a common low-loss Si_3N_4 platform yet separately fabricated. Initially the two PICs are characterized, revealing a 3 dB channel-bandwidth of around 0.6 nm for the ROADM within a 2.55 dB FtF loss-budget in the 1550 nm region, which is compensated by the on-chip net-gain provided by the EDWA. Proof-of-principle lossless ROADM operation is verified at up to 240 Gb/s WDM capacity, successfully routing 4λ × 60 Gb/s channels to its four Drop ports. Bit Error Rate (BER) measurements confirm successful operation at 25 Gb/s with 1.9 dB average penalty. The performance of the proposed ROADM architecture is also benchmarked in a two-stage optical bus with 4×25 Gb/s WDM traffic, comprising the proposed Si_3N_4 EDWA-ROADM and a second Si_3N_4-ROADM spaced by 10 km of fiber, selectively dropping two wavelengths at the first stage and the other two wavelengths at the second stage with a spectral suppression ratio higher than 12 dB between the desired channel and any other channel. To the authors' knowledge, this is the first all-silicon lossless ROADM operation, paving a roadmap for monolithically co-integrating EDWAs and MZI-switches on the same Si_3N_4 platform for scalable switching matrices.

The paper organized as follows: Part II describes the design and characterization of the ROADM and EDWA PICs, Part III presents the 4×25 Gb/s WDM routing across a 10 km two-stage bus, Part IV covers 60 Gb/s operation prior to the conclusions.

II. Photonic Integrated Circuits

Co-integrating EDWAs and ROADMs on a SiPho platform can potentially realize a lossless, monolithically integrated switch. A schematic illustration of an envisioned lossless ring network is shown in Fig. 1, including EDWA-based pre-amplification and 1×4 wavelength routing, replacing the bulky yet widely-used EDFA and MEMS-based components. The PIC prototypes developed are coupled together externally through fiber-patchcords for this proof-of-principle, and are here initially described and characterized in this section.

A. Low Loss Si_3N_4 ROADM

The ROADM relies on a Si_3N_4/SiO_2 TriPleX platform with low losses below 0.1 dB/cm [39]. The chip layout adopts a configuration of a nested MZI-interleaver with two cascaded interleavers per arm, as shown in Fig. 2(a), for a total of six dual-MZI components. Each of the six interleavers relies on the same generic configuration of a dual cascaded asymmetric MZI lattice-filter as shown in Fig. 2(b), where the first MZI-stage has double (2ΔL) the differential waveguide path-length of the first MZI stage (ΔL), which finally determines its Free Spectral Range (FSR). For an FSR of 200 GHz (grey-colored MZIs), the short differential waveguide path-length, ΔL, of the first MZI stage is ΔL_1=872.1 μm, while for an FSR of 400 GHz (the

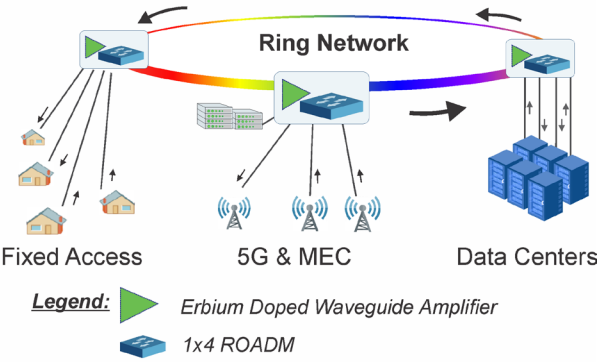

Fig. 1. Schematic of a WDM ring network of three lossless ROADMs monolithically co-integrating an Erbium Doped Waveguide Amplifier (EDWA) on Si_3N_4.

orange-colored MZIs) a path-length of ΔL_2=436 μm is used. Tunable thermo-optic couplers allow to accurately define the splitting ratio between the branches of each MZI, which are indicated with the k_1, k_2 and k_3 coefficients, and fine-tune the shape of the filter spectral response. Two Phase Shifters, *PS1* and *PS2*, are placed inside the arms of the two MZIs, to allow adjusting the wavelength-positions of the maximum and minimum signal-interference of the filter, so as to drop or pass through the desired wavelength at the ROADM output ports.

The current layout-design supports adding or dropping four wavelengths in the C-band, as described with the colored arrows in Fig. 2(a). Four wavelengths spaced by 100 GHz of an incoming 4λ-WDM stream are initially divided into pairs of odd (blue λ_1 and black λ_3) and even (red λ_2 and green λ_4) wavelengths by the first grey-colored MZIs with 200 GHz FSR, that propagate to the upper and lower arms of the ROADM. The wavelength pairs are further subdivided at each separate wavelength by the nested orange-colored MZIs with an FSR of 400 GHz. The designed transfer function of the dual-MZI interleaver is shown at the left and right inset of Fig. 2(b), corresponding to $\Delta L_1 = 872.1$ μm and $\Delta L_2 = 436$ μm for a differential waveguide path-length at the first MZI-stage of the orange- and grey-colored MZIs respectively. Consequently, each of the four 100 GHz spaced WDM channels can be finally routed at a separate drop output port or propagate to the Through port. Each MZI filter was designed targeting flat-top pass-band response [13], while the fabricated PIC is assembled on an electro-optic PCB with Temperature Control (TEC) and housed in a bench-top solution, as shown in in Fig. 2(c).

Initially, we identified the optimal operational settings of ROADM to configure a routing state with all four wavelengths being dropped at its four outputs and characterized its spectral response and channel bandwidths. For this purpose, the input port of ROADM was powered by the Amplified Spontaneous Emission (ASE) noise of an EDFA, while capturing the spectrum at an Optical Spectrum Analyzer (OSA). The four captured spectra being color-coded according to the previous description and overlapped together are plotted in Fig. 2(e), achieved for coupling coefficients of k_1=0.9248, k_2 = 0.280 and k_3 = 0.500. The output spectra exhibit a 3-dB channel bandwidth of 0.66 nm and a static crosstalk lower than -18 dB. Having configured properly the routing state, we characterized its FtF loss by centering the Continuous Wavelength (CW) of a Tunable Laser Source (TLS) at the peak-center of each channel and measuring its optical output power. The average FtF losses between three of the Drop output ports, namely Drop 2-4, were measured to be 2.55 dB, while Drop 1 featured some additional loss due to non-ideal patch-cord at the fiber-array. The FtF loss is further attributed to 0.6 dB propagation loss for the longest on-chip path of 58.2 mm and 0.975 dB/facet coupling loss for each of the fiber-to-Si_3N_4 interface.

B. Monolithic Integrated EDWA

Fig. 3(a) depicts a schematic of the EDWA, comprising an $Al_2O_3:Er^{3+}$ active region in a spiral waveguide and input and output Si_3N_4 passive waveguides, marked with brown and blue color respectively. The Si_3N_4 waveguide layer was designed to host two fiber-to-Si_3N_4 coupling waveguides for the signal and pump wavelengths followed by an on-chip MMI for multiplexing purposes, which was not however used in our

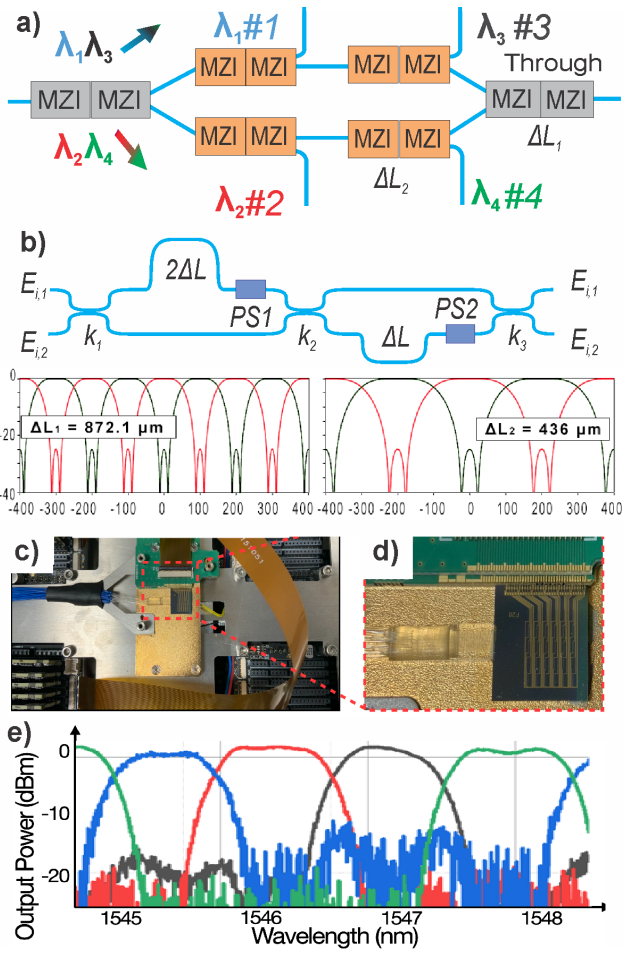

Fig. 2. (a) Circuit layout of the Si_3N_4 ROADM based on nested MZI interleavers, (b) design of the generic dual MZI filter and its transfer function for a differential length of ΔL_1=872.1 μm (left inset) and ΔL_2=436 μm (right inset) used in the orange- and grey-colored MZIs respectively, (c) photos of the packaged device, (d) microscope image and (e) transfer function of the four drop ports of the ROADM

experiment, as will be described later in the text, and an adiabatic coupler for coupling the light to the $Al_2O_3:Er^{3+}$ layer. After the spiral waveguide amplifier similar components are placed symmetrically.

The EDWA chip was fabricated following the process described in [35], using low-pressure chemical vapor deposition (LPCVD) of a 200 nm thick Si_3N_4 layer, patterned to a 1.4 μm width using i-line contact lithography, followed by Reactive Ion Etching (RIE) to produce a 1.4 μm×200 nm waveguide core with measured propagation losses of 0.12 dB/cm at 1550 nm [36]. A SiO_2 film was deposited above the Si_3N_4 layer by LPCVD, followed by $Al_2O_3:Er^{3+}$ layer deposition with 800 nm thickness by RF reactive co-sputtering and a targeted Er^{3+} concentration of 1.7×10^{20} cm^{-3}. The Al_2O_3 waveguides were then patterned by i-line lithography and etched using RIE [35], forming a cross-section of 1.4 μm×800 nm.

The EDWA was initially characterized in pump-probe measurements at a probe-station to test its signal-enhancement capabilities, transmitting four wavelengths with the pump-light on and off. Initially a fiber array was employed to separately couple the signal and pump light at the respective ports of the EDWA PIC, using diphenyl ether index matching gel to

This article has been accepted for publication in a future issue of this journal, but has not been fully edited. Content may change prior to final publication. Citation information: DOI 10.1109/JLT.2021.3131130, Journal of Lightwave Technology

minimize the fiber-coupling losses. However, due to evaporation of the gel, there were instabilities in the probe-station setup resulting in temporal misalignments of the fiber array to the signal and pump ports of the EDWA. For this reason, the signal and pump lights were optically multiplexed externally using a fiber-pigtailed WDM coupler, before being simultaneously launched through a Polarization Maintaining (PM) fiber with FC/PC connector via butt-coupling at the pump port only, and without performing any multiplexing at the on-chip MMI. The test setup and a microscope image of the pumped $Al_2O_3:Er^{3+}$ spiral waveguide are depicted in Fig. 3(b), showing the characteristic green light emission of the active region generated by the excited erbium ions. An SEM image of the tapered tip of the adiabatic coupler is shown at the inset. The estimated losses of the two input/output interfaces for coupling the signal in the C-band and pump light at 980 nm were 10 dB and 12 dB respectively. The MMI losses for the signal light were calculated around 1.7 dB for signal port and 8.3 for the pump port in the C-band. The adiabatic coupler exhibited 0.5 dB losses per transition between the $Al_2O_3:Er^{3+}$ and Si_3N_4. The design and fabrication of the components are described in more detail in [35]-[37].

In this experiment, four C-band signals generated by four TLSs were optically multiplexed and coupled externally together with the 980 nm pump light using a 1550 nm/980 nm WDM coupler, before being simultaneously launched through a single fiber-tip at the pump port of the EDWA. The overall coupling from the single fiber-tip to the active region of the EDWA added up to an estimated aggregate signal loss of 18.8 dB, while the output signal was collected from the signal port with 12.2 dB aggregate losses from the EDWA active region to the fiber. For the pump-probe characterization, the optical power level of the 4λ-WDM signals was tuned across a dynamic range of 15 dB, from -3 dBm up to 12 dBm measured at the fiber tip, allowing to monitor a light- and heavily-saturated EDWA-gain condition, while the 980 nm pump featured an average power of 24.7 dBm. The output of the EDWA was captured at an OSA, to evaluate the signal enhancement in the WDM transmission with the 980 nm pump light on and off.

Figure 3(c) shows the recorded spectra of four wavelengths, when the pump light was On and Off, marked with red and black color respectively, overlapped for comparison purposes. Four distinct cases of incident input signal power levels of -3 dBm, 2 dBm, 7 dBm and 12 dBm are shown. As it can be seen in the upper left spectrum, for a -3 dBm input power in the light saturation regime, all four red-plotted signals (i.e., pump on) are enhanced by 15 dB on average compared to the four black-colored signals (i.e., pump off). Equivalently, for the heavily saturated gain regime at the lower left spectrum for a 12 dBm incident input signal power, the signals in the red plot of the spectrum (i.e., pump on) are enhanced by 5.7 dB on average compared to the black plot of the spectrum (i.e., pump off). Although for the four cases, the signal enhancement at the signal peaks were 15 dB, 13.16 dB, 9.27 dB and 5.7 dB respectively, the baseline of the optical spectrum exhibit differences of 4.22 dB, 4.03 dB, 3.05 dB and 2.54 dB between the red- and the black-plots, as marked in Fig. 3(c), which refer to the ASE noise generated by the EDWA. When the pump is On (red-plots) with an average incident signal power of

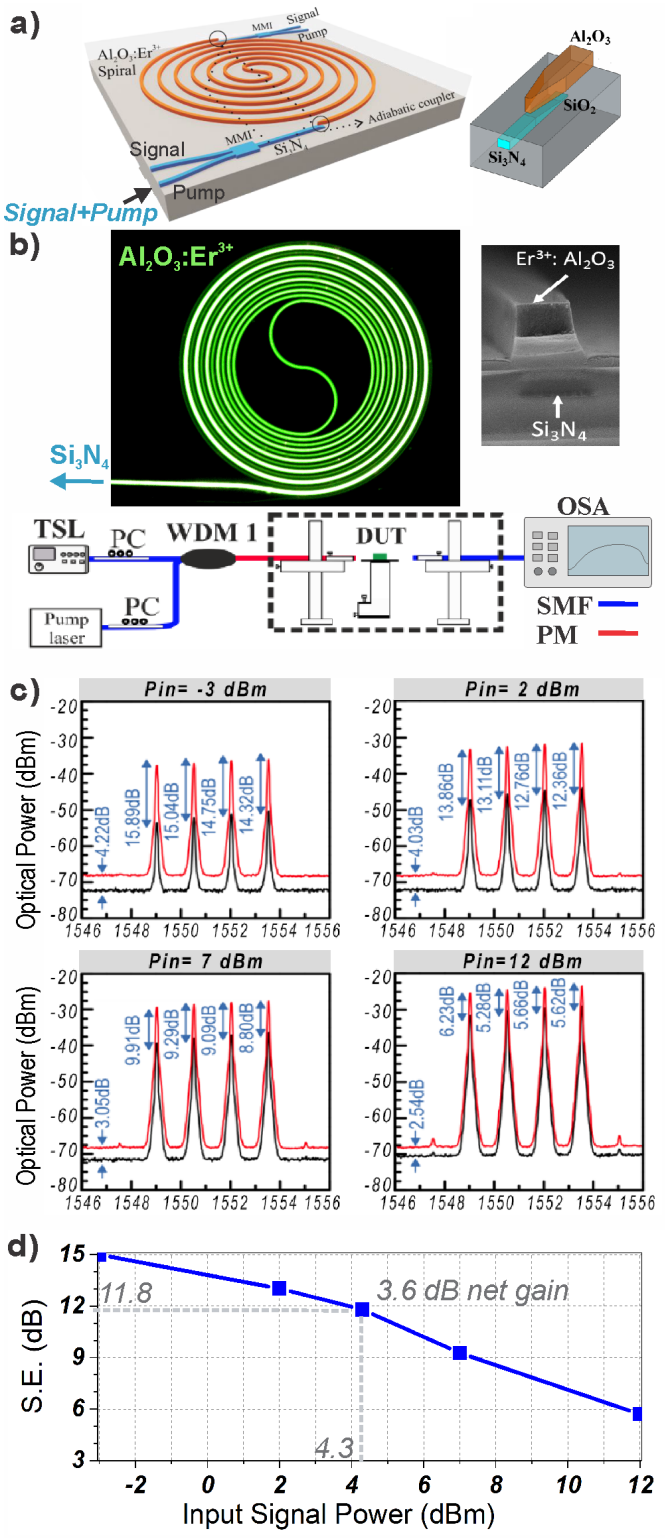

Fig. 3 (a). Schematic of the $Al_2O_3:Er^{3+}$ waveguide with Signal and Pump inputs at left facet, followed by the Mux MMI, the adiabatic coupler and the Al_2O_3 waveguide, with the adiabatic taper shown at the inset, (b) characterization setup and microscope image of the EDWA when powered by pump light and SEM image of the tapered coupling region, (c) Optical spectra of the signal enhancement at the peaks of the of 4λ-WDM channels with total input power of -3 dBm up to 12 dBm during pump on (red plot) and pump off (black plot), values of the amplified spontaneous emission (ASE) background indicated at the baseline, (d) Plot of the Signal Enhancement (SE) versus transmitted optical power.

24.7 dBm, the spectra of the ASE power equals to that of the background, being constantly equal to -68 dBm. A more detailed characterization of the EDWA ASE noise at different power-levels of the pump light can be found in [35].

The curve of the average signal enhancement versus the transmitted power is plotted in Fig.3(d). As expected, the values reveal greater signal enhancement for lower signal input powers with less saturation of the gain. By adjusting the input signal to even lower power levels or tuning the signal wavelengths closer to the 1530 nm region, the EDWA inherently provides greater amplification values and signal enhancement up to 30 dB could easily be recorded [35]. However, the current work focuses at 1550 nm wavelength region, where an incident signal power of 4.3 dBm experienced a signal enhancement of 11.8 dB, as can be seen in the plot of Fig. 3(d). Yet, the estimation of the net-gain has to be based on the actual signal output power, minus the input signal power of the EDWA PIC, minus the coupling loss from the fiber till the $Al_2O_3:Er^{3+}$ active region both at the input as well as the output sides of the amplifier. As the signal absorption plus propagation losses at 1550 nm were measured as 1.4 dB/cm for the utilized level of input signal, a measured EDWA net-gain of 3.6 dB, corresponding to 0.6 dB/cm gain, was obtained for the current setup.

Although gain-amplification values greater than 1.4 dB/cm and up to 18 dB net-gain have been experimentally measured in previous evaluations of similar $Al_2O_3:Er^{3+}$ EDWAs, the obtained 3.6 dB net-gain is sufficient for our proof-of-concept demonstration of a lossless Si_3N_4 ROADM. In case of a single EDWA-ROADM device that would monothically integrate both the EDWA and the ROADM in one PIC, this net-gain would suffice to compensate the 2.55 dB FtF losses of the ROADM, including 1.95 dB for the two fiber-to-Si_3N_4 interfaces (0.975 dB/facet) and 0.6 dB on-chip propagation losses, as well as the additional 1 dB loss for the two Si_3N_4-to-EDWA adiabatic couplers. Yet, the overall net–losses of the EDWA PIC itself were -27.4 dB.

III. Lossless ROADM with 240 Gb/s WDM Capacity

In this section, the two PICs are combined in a proof-of-concept demonstration of the lossless wavelength-routing of a 4λ WDM data stream with up to 240 Gb/s traffic-capacity.

A. Experimental Setup and Power Budget estimation

The complete experimental setup used for the evaluation of the proposed concept is shown in Fig. 4(a). Four DFB laser sources tunable in the C-band were used to generate four CW signals with 100 GHz channel spacing, centered at λ1-λ4 wavelength of 1549.6 nm, 1550.4 nm, 1551.2 nm and 1552 nm, marked with blue, red, black and green color. The four CWs were optically multiplexed by an Arrayed Waveguide Grating (AWG) multiplexer, whose output was propagated to an EDFA and $LiNbO_3$ MZI for modulation, generating four data streams of -1.7 dBm per channel and aggregate optical power of 4.3 dBm. Tuning of the power levels was controlled by a Variable Optical Attenuator (VOA). The operation of the $LiNbO_3$ modulator was driven by a 2^7-1 Pseudo Random Bit Sequence (PRBS) that was generated by the electrically amplified output of a 25 Gb/s programmable Pulse Pattern Generator (PPG). This allowed imprinting the PRBS data-pattern on the 4λ CWs, to generate a WDM data-traffic with aggregate throughput of 100 Gb/s (4×25Gb/s).

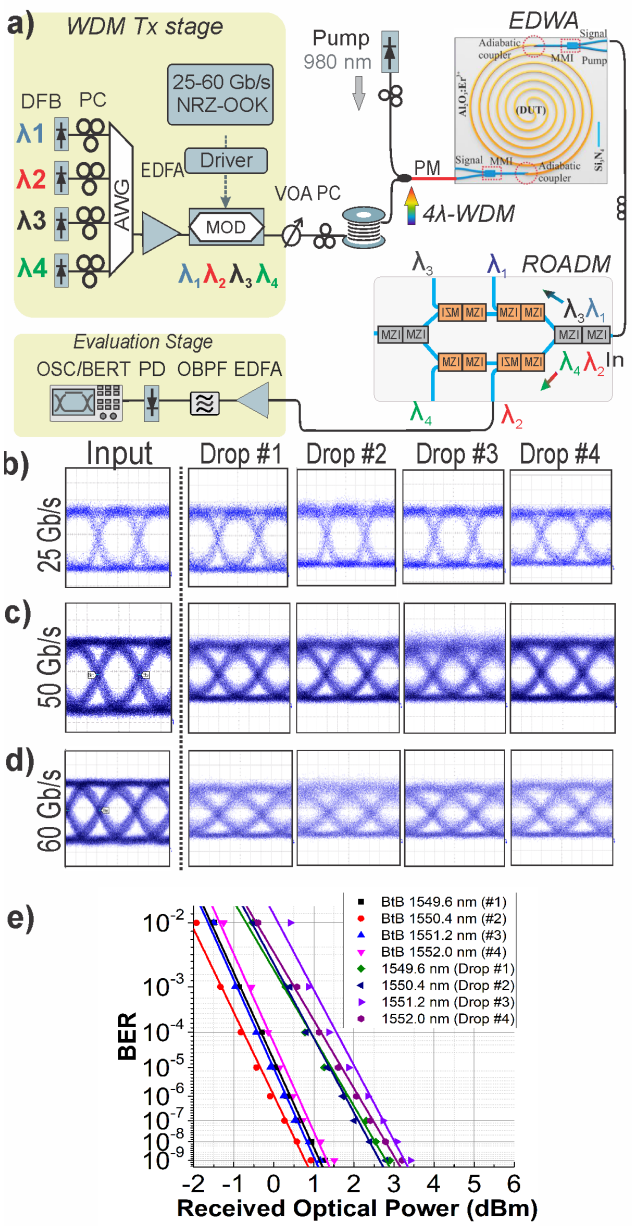

Fig. 4 a) Experimental setup used for the lossless wavelength-routing at 4×25 Gb/s, 4×50 Gb/s and 4×60 Gb/s, DFB: Distributed Feedback Grating, PC: Polarization Controller , PM: Polarization Maintaining fiber, OBPF: Optical Bandpass Filer, λ1-λ4: 1549.6 nm, 1550.4 nm, 1551.2 nm, 1552 nm. b) Eye diagrams for the input and four Drop output signals at 4×25 Gb/s, c) 4×50 Gb/s and d) 4×60 Gb/s, and e) Bit Error Rate (BER) curves of the four 25 Gb/s Drop signals and Back-to-Back configuration.

Following the generation of the signals, the WDM data-stream was transmitted through a few hundred meters of Single Mode Fiber (SMF) to partially de-correlate the data-patterns, before being fed to the C-band input port of a WDM (1550/980 nm) fiber coupler. The other port of the WDM coupler was connected to a pump light obtained by a DFB laser emitting in the 980 nm region, combining the 4λ-WDM data stream with the pump light. The output of the WDM coupler was in-turn connected at a PM fiber for simultaneous pump and signal transmission to the EDWA through its input pump port using butt-coupling scheme. The PM was attached to a micro-

positioner, to launch the signals to the EDWA PIC, that was placed on the vacuum chuck of the chip-characterization stage. This setup with one PM coupled to the pump port was used instead of one array of two fibers coupled separately to the signal and the pump port, as it proved more stable for longer experimental time. Polarization Controllers (PCs) were used to handle the polarization of the signals.

The emitted output of the EDWA was collected by the signal output port at the right facet, using another fiber probe-tip placed at a second micro-positioning alignment stage. The 4λ-WDM output data signals, after being amplified by the EDWA were propagated to the fiber-pigtails of packaged Si_3N_4 ROADM. Upon entering the ROADM through its input port, the data traffic got demultiplexed to its four individual wavelengths through the cascaded wavelength-filtering operation of the dual-MZIs with 100 GHz spacing. Each of the demultiplexed wavelength-channels appeared at one of the four Drop output ports, and after filtering of any remaining pump or ASE noise, were measured in terms of optical power to evaluate the link power-budget before being driven to the evaluation stage for monitoring purposes.

Using the above setup, we initially measured the received optical power reaching the evaluation stage for each of the wavelength-channels, after being propagated through the EDWA and demultiplexed by the ROADM, using a power meter. By transmitting all four wavelengths with a -1.7 dBm per channel, the average optical power of the signals appearing at the Drop output ports 2-4 was -32.5 dBm per channel. The measurements reveal an end-to-end power budget of 30.8 dB, stemming from the 27.4 dB net-loss by the EDWA PIC, 2.55 dB by the FtF ROADM loss and the rest attributed to the fiber patch-cord interconnecting the two PICs. Although the use of two discrete PICs degraded the power budget of this setup, excluding the high passive coupling losses of 30 dB by the EDWA PIC (i.e., 18.3 dB for fiber-to-Si_3N_4 and 11.7 dB for the Si_3N_4–to-fiber), which can be drastically reduced by utilizing fiber-to-waveguide mode converters at the input and output ports of the device, and the 0.8 dB by the EDWA-ROADM inter-connecting patch-cord, lossless operation was achieved. In case of a fully integrated EDWA-ROADM on a single Si_3N_4 PIC, lossless operation would require an optical power of -20.975 dBm per channel, i.e. -1.7 dBm measured channel power minus 18.3 dB and 0.975 dB of the coupling stages, to achieve equivalent EDWA gain regime.

B. Lossless wavelength routing of 240 Gb/s data traffic

Having appropriately configured the EDWA gain and the ROADM state, several data transmission experiments were performed, to validate the capability of the proposed device to route high capacity WDM data traffic. In particular, three transmission scenarios at 4×25 Gb/s, 4×50 Gb/s and 4×60 Gb/s data traffic were performed, resulting in an aggregate WDM traffic of 100 Gb/s, 200 Gb/s and 240 Gb/s. When performing data transmissions through the developed setup, the transmitted optical signal was set at -1.7 dBm per channel. At the final evaluation stage, additional EDFA and Optical Bandpass Filter (OBPF) had to be employed, to increase the signal-power, in order to be detected at a photoreceiver for o/e conversion and be captured at an Optical Sampling Scope (OSC) and Bit Error Rate (BER) testing equipment.

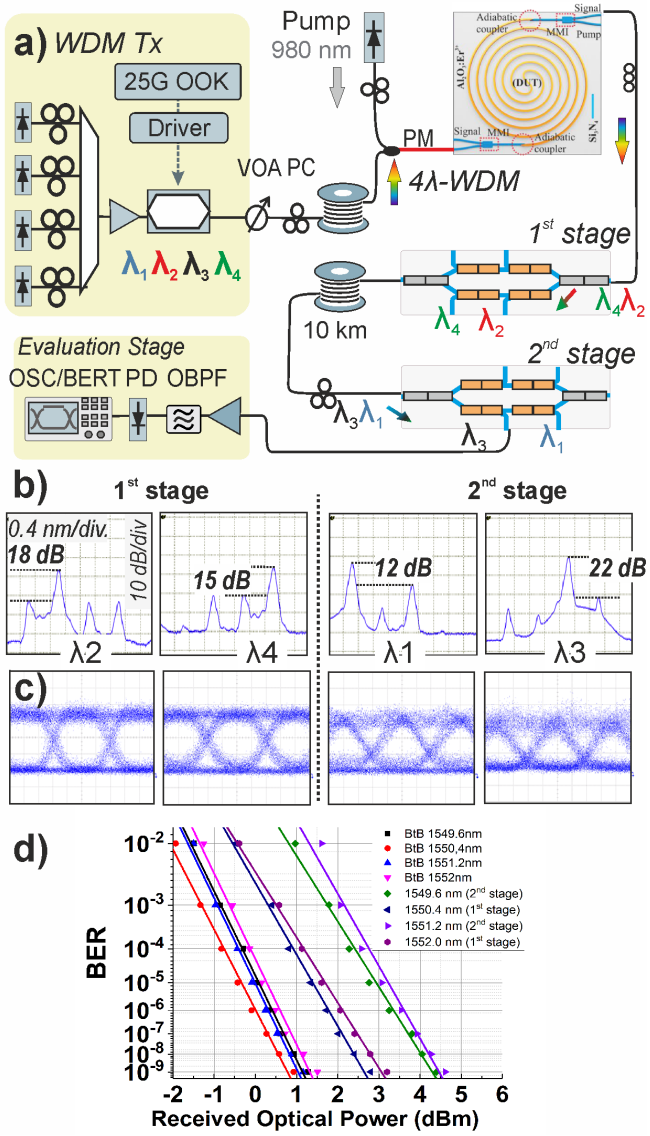

Fig. 5 a) Experimental setup of a two-stage bus, including an EDWA ROADM node and a second ROADM spaced by 10 km fiber with experimental results for λ2 and λ4 dropped at the 1st stage and λ1 and λ3 dropped at the 2nd stage, b) output spectra and c) eye diagrams for each Drop signal output and d) Bit Error Rate (BER) measurements for the four signals.

The eye diagrams of the input signal and the four Drop output signals for the 4×25 Gb/s, 4×50 Gb/s and 4×60 Gb/s are shown in Fig. 4(b), (c) and (d). The measurements reveal that all four wavelengths were successfully demultiplexed by the ROADM, achieving open eye diagrams for all output signals. For the 25 Gb/s linerate, an Extinction Ratio (ER) of around 10.1 dB was recorded and an Amplitude Modulation (AM) of less than 0.9 dB with no serious degradation compared to the input signal. On the other hand, higher data rates of 50 Gb/s and 60 Gb/s also passed through the ROADM. Despite the some small filtering effect being observed, the ER of the received signal was still measured to be greater than 4.5 dB for all cases.

Finally, the performance of the proposed lossless ROADM was benchmarked using BER measurements for the 4×25 Gb/s

operational setup. All four wavelength channels were evaluated either at the Drop output ports or in Back-to-Back (BtB) configuration at the input of the EDWA. The BER curves have been plotted in Fig. 4(e). Error free operation at the 10^{-9} operating condition was achieved for all wavelength channels with an average BER penalty of 1.8 dB. Despite some variations in the slopes of the BER curves of the WDM channels, attributed to the drifting of the modulator bias, cascaded ASE noises and slightly different transfer functions of the ROADM channels during the measurements, the worst BER penalty recorded was less than 2.4 dB for Drop 3.

IV. Two Stage Optical BUS including Two ROADMs

The performance of the envisioned ROADM node was also benchmarked a realistic two stage optical bus topology, using the experimental setup shown in Fig. 5(a). Specifically, the previous setup with an EDWA placed before the ROADM was further extended with the introduction of a 10 km SMF, the output of which is connected to a second Si_3N_4 ROADM without EDWA. The lossless condition was maintained only for the first stage, owing to the presence of one EDWA PIC, while the main target was to evaluate the capability to route high-bandwidth signals in longer distance transmissions setups and cascaded operation. The setup hosts four reconfigurable non-dispersion compensated optical links, which can be selectively dropped at the output ports of the first ROADM stage or at the second ROADM at a linerate of 25 Gb/s.

The two ROADMs were properly configured to route two wavelengths, namely λ2 and λ4, at the first stage, and the remaining two wavelengths λ1 and λ3 to the second ROADM stage, where they were dropped to the respective ports 1 and 3, as shown in Fig.5(a). The performance of the two stage configuration in routing the 4λ-WDM traffic was evaluated by capturing all output spectra at an OSA, which are shown in Fig. 5(b). As it can be seen in the four spectra recorded at Drop 2 and 4 of the first stage and Drop 1 and 3 of the second stage, a spectral suppression ratio of 18 dB, 15 dB, 12 dB and 22 dB was achieved when demultiplexing each channel.

In order to further validate the performance of the two stage optical bus, data transmissions and BER measurements were performed, recording the eye diagrams at the four Drop ports. The eye diagrams are shown in Fig. 5(c), being wide open with equivalent high ER as in the previous section for λ2 and λ4 signals of the first stage. On the other hand, λ1 and λ3 also exhibited open eye diagrams, featuring a Gaussian-shaped profile, owing to the impact of chromatic dispersion of the 10 km long fiber. BER measurements performed on the received eye diagrams are plotted in the curves of Fig. 5(d). All four Drop signals achieved error free operation at the 10^{-9} condition, with 1.8 dB BER penalty for the first EDWA-ROADM stage and an additional 1.7 dB BER penalty for the second stage, verifying the capability of the node to handle cascaded layouts and long-distances of optical networks.

V. Conclusion

A lossless ROADM node relying exclusively on silicon photonics was experimentally presented for the first time. The proposed device is based on an MZI-based lattice-filter layout and a 5.9 cm-long $Al_2O_3:Er^{3+}$ EDWA monolithically integrated on a Si_3N_4 platform. Although the current work relies on two discrete PICs to demonstrate the proof of principle operation, it indicates a possible roadmap towards monolithically co-integrating EDWA and rare-earth gain-elements together with larger-port count photonics switching matrixes on a single PIC for a range of lossless photonic switching matrix applications, including programmable photonic processors or even lidars, as part of future work [40]. Such a lossless photonic switching subsystem could form a highly functional and cost-effective PIC solution for 5G fronthaul and access networks, while extending its cascadability to higher number of components, e.g., two ROADMs, without compromising the total insertion losses can potentially form the basis for larger-size functional ROADMs and OCSs for Telecom and Datacom sectors.

References

[1] P. J. Winzer, D. T. Neilson, and A. R. Chraplyvy, "Fiber-optic transmission and networking: the previous 20 and the next 20 years," *Opt. Express,* vol. 26, no. 18, pp. 24190–24239, 2018

[2] D. Evans, "The Internet of Things How the Next Evolution of the Internet Is Changing Everything,"April 2011, Cisco Internet Business Solutions Group, White Paper

[3] W. Shi, Y. Tian, A. Gervais, "Scaling capacity of fiber-optic transmission systems via silicon photonics," *Nanophotonics,* vol. 9, no. 16, pp. 469292-4663, Oct 2020

[4] B. Lee, et. al. "Monolithic silicon integration of scaled photonic switch fabrics, CMOS logic, and device driver circuits," *IEEE J. of Lightwave Technology*, vol. 32, no. 4, pp. 743-751, Feb. 2014

[5] M. Vasilyev and S. Radic, "Optical Amplifiers," in *Springer Handbook of Optical Networks*, New York, NY, USA; Springer, 2020, ch. 3, pp. 51–81

[6] D. Marom, et. al., "Survey of Photonic Switching Architectures and Technologies in Support of Spatially and Spectrally Flexible Optical Networking [Invited]," *IEEE/OSA J. Opt. Commun. Netw*., vol. 9, no. 1, Jan. 2017

[7] R. Konoike, et. al. "SOA-Integrated Silicon Photonics Switch and Its Lossless Multistage Transmission of High-Capacity WDM Signals," *IEEE. J. Lightwave Technology*, vol. 37, no. 1, pp.123-130, Jan. 2019.

[8] Q. Chang, S. Rumley, M. Bahadori, K. Bergman, "Photonic switching in high performance datacenters [Invited]," *Optics Express,* vol. 26, no. 12, pp.16022-16043, June 2018

[9] Y. Li, Y. Zhang, L. Zhang, A. Poon, "Silicon and hybrid silicon photonic devices for intra-datacenter applications: state of the art and perspectives [Invited]," *Photonics Research,* vol. 3, no. 5, pp. B10-B27, Oct. 2015

[10] S. Nakamura, S. Yanagimachi, H. Takeshita, A. Tajima, T. Hino and K. Fukuchi, "Optical Switches Based on Silicon Photonics for ROADM Application," in *IEEE J. of Selected Topics in Quantum Electronics,* vol. 22, no. 6, pp. 185-193, Nov.-Dec. 2016

[11] B. Skubic, et. al. "Rethinking Optical Transport to Pave the Way for 5Gand the Networked Society," *IEEE J. Lightwave Technology*, vol. 33, no. 5, pp. 1084-1091, Mar. 2015

[12] A. Tsakyridis, et. al. "Reconfigurable Fiber Wireless IFoF Fronthaul with 60 GHz Phased Array Antenna and Silicon Photonic ROADM for 5G mmWave C-RANs," *IEEE J. Selected Areas in Communications*, early access

[13] C. Mitsolidou, et. al. "A 5G C-RAN Optical Fronthaul Architecture for Hotspot Areas Using OFDM-Based Analog IFoF Waveforms," *Applied Sciences,* vol. 9, no. 9, 4059, Sep. 2019

[14] C. Browning, et. al. "A Silicon Photonic Switching Platform for Flexible Converged Centralized-Radio Access Networking," *IEEE J. Lightwave Technology,* vol. 38, no. 19, pp. 5386-5392, Oct 2020

[15] V. Sorianello, et. al., "Polarization insensitive silicon photonic ROADM with selectable communication direction for radio access networks," *Optics Letters*, vol. 41, pp. 5688-5691, 2016

[16] B. Lee, N. Dupuis, "Silicon Photonic Switch Fabrics: Technology and Architecture," *IEEE J. Lightwave Technology*, vol. 37, no. 1, pp. 6-20, Jan 2019

[17] P. Dumais, et. al. "Silicon Photonic Switch Subsystem With 900 Monolithically Integrated Calibration Photodiodes and 64-Fiber Package," *IEEE J. Ligtwave Technology*, vol. 36, no. 2, pp. 233-238, Jan. 2018

[18] A. Wonfor, H. Wang, R. Penty, I. White, "Large Port Count High-Speed Optical Switch Fabric for Use Within Datacenters [Invited]," *OSA J Optical Communc. and Networking*, vol. 3, no. 8, pp. A32-A39, July 2011

[19] D. Thomson et al., "Roadmap on silicon photonics," *IOP J. Opt.*, vol. 18, Art. no. 073003, 2016.

[20] N. Margalit, et. al., "Perspective on the future of silicon photonics and electronics," *Appl. Phys. Lett*., vol. 118, 220501, June 2021

[21] T. Kirihara, M.Ogawa, H. Inoue, H. Kodera, K. Ishida, "Lossless and Low-Crosstalk Characteristics in an InP-Based 4x4 Optical Switch with Integrated Single-Stage Optical Amplifiers," *IEEE Photon. Tehcnology Letters*, vol. 6, no. 2, pp. 218-221, Feb. 1994.

[22] Y. Kai, et. al. "A compact and lossless 8 × 8 SOA gate switch subsystem for WDM optical packet interconnections," *ECOC,* Brussels, Belgium, Sep. 2008.

[23] Q. Cheng, A. Wonfor, J. L. Wei, R. V. Penty, I. H. White, "Demonstration of the feasibility of large-port-count optical switching using a hybrid Mach–Zehnder interferometer–semiconductor optical amplifier switch module in a recirculating loop," *Optics Letters,* vol. 39, no. 18, pp. 5244-5247, Sep. 2014.

[24] K. Prifti, et. al. "Lossless Photonic Integrated Add-Drop Switch Node for Metro-Access Networks," *IEEE Photonics Technology Letters*, vol. 32, no 7, pp. 387-390, Feb. 2020.

[25] D. W. Feyisa, et. al. "140 Gb/s WDM Data Routing in a Lossless Strictly Non-Blocking SOA-Based Photonic Integrated 8×8 Space Switch," *OFC*, virtual, Mar. 2021

[26] N. Dupuis, et. al. "A 4×4 electrooptic silicon photonic switch fabric with net neutral insertion loss," *IEEE J. Lightwave Technology*, vol. 38, no. 2, pp. 178-174, Jan. 2020

[27] H. R. Mojaver, et. al. "Lossless Operation of an 8 × 8 SiPh/InP Hybrid Optical Switch," *IEEE Photonics Technology Letters,* vol. 32, no. 11, pp. 667-670, June 2020

[28] H. R. Mojaver, et. al. "High Radix SOA-Based Lossless Optical Switch Prototyping for 25 GBaud PAM4 Transmission in Modern Intra-datacenter Applications," *OFC,* virtual, March 2021

[29] T. Komljenovic, et. al. "Heterogeneous silicon photonic integrated circuits," *IEEE J. Lightwave Technology*, vol. 34, no. 1, pp. 20-35, Jan. 2016

[30] J. M. Ramirez, "III-V-on-Silicon Integration: From Hybrid Devices to Heterogeneous Photonic Integrated Circuits," *IEEE J. Selected Topics in Quantum Electronics,* vol. 26, no. 2, aID 6100213, March 2020

[31] T. Matsumoto, et. al. "Hybrid-Integration of SOA on Silicon Photonics Platform Based on Flip-Chip Bonding," *IEEE J. Lightwave Technology,* vol. 37, no. 2, pp. 307-313, Jan.2019

[32] D. Fitsios, et. al. "Dual SOA-MZI Wavelength Converters Based on III-V Hybrid Integration on a -Scale Si Platform," *IEEE Photonics Technology Letters,* vol. 26, no. 6, pp. 560-563, Mar. 2014

[33] A. Wonfor, et. al. "Control architecture for high capacity multistage photonic switch circuits," *J. Opt. Networking*, vol. 6, no. 2, pp. 180-188 , Feb. 2007

[34] J. D. B. Bradley, M. Pollnau, "Erbium-doped integrated waveguide amplifiers and lasers," *Laser Photonics Rev.*, vol. 5, no. 3, pp. 368, 2011

[35] J. Mu, M. Dijkstra, J. Korterik, H. Offerhaus, S. M. Garcia-Blanco, "High-gain waveguide amplifiers in Si_3N_4 technology via double-layer monolithic integration," *Photonics Res.,* vol. 8, no. 10, pp. 1634-1641, Oct. 2020.

[36] J. Mu, S. A. Vázquez-Córdova, M. A. Sefunc, Y.-S. Yong, S. M. García-Blanco, "A low-loss and broadband MMI-based multi/demultiplexer in Si3N4/SiO2 technology," *J. Lightwave Technol.*, vol. 34, no. 15, pp. 3603-3609, Aug. 2016

[37] J. Mu, M. Dijkstra, Y. Yong, M. de Goede, L. Chang, and S. M. García-Blanco, "Monolithic integration of Al_2O_3 and Si_3N_4 toward double-layer active-passive platform," *IEEE J. Sel. Top. Quantum Electron*. 25, vol. 25, no. 5, 8200911, Sept.-Oct. 2019

[38] J. Bradley, et. al. "170 Gbit/s transmission in an erbium-doped waveguide amplifier on silicon," *Optics Express*, vol. 17, no. 24, pp. 22201-22208, Nov 2009

[39] C. Roeloffzen, et. al. "Low-Loss Si_3N_4 TriPleX Optical Waveguides: Technology and Applications Overview", *IEEE J. Selected Topics in Quantum Electronics,* vol. 24, no. 4, 2018

[40] OPHELLIA EU Project, https://lidar-ophellia.eu